

# Differentiation trajectories and biofunctions of symbiotic and un-symbiotic fate cells in root nodules of *Medicago truncatula*

Qinyi Ye<sup>1,2,3</sup>, Fugui Zhu<sup>1,3</sup>, Fanghao Sun<sup>1,3</sup>, Tai-Cheng Wang<sup>1</sup>, Jiale Wu<sup>1</sup>, Peng Liu<sup>1</sup>, Chen Shen<sup>1</sup>, Jiangli Dong<sup>1,\*</sup> and Tao Wang<sup>1,\*</sup>

<sup>1</sup>State Key Laboratory of Agrobiotechnology, College of Biological Sciences, China Agricultural University, Beijing 100193, China

<sup>2</sup>College of Grassland Science and Technology, China Agricultural University, Beijing 100193, China

<sup>3</sup>These authors contributed equally to this article.

\*Correspondence: Jiangli Dong (dongjl@cau.edu.cn), Tao Wang (wangt@cau.edu.cn)

<https://doi.org/10.1016/j.molp.2022.10.019>

## ABSTRACT

The root nodule is a complex symbiotic nitrogen fixation factory, in which cells are highly heterogeneous. However, the differentiation trajectories and interconnection of nodule cells remain largely unknown. In this study, we set up a modified protocol for nodule protoplast preparation and performed a single-cell RNA sequencing profiling of the indeterminate *Medicago truncatula* nodule. We designated 13 cell clusters with specific expression patterns in 14-day post inoculation nodules and constructed a spatial and functional cellular map based on experimental data and bioinformatic analyses. Pseudotime analysis further revealed that two groups of apical meristematic cells develop into symbiotic and un-symbiotic fate cells along their particular trajectories. Biofunction analysis of each cell cluster revealed their particularity and interrelation, especially that the un-infected cells in nitrogen fixation zone are also involved in nitrogen assimilation by undertaking the asparagine synthesis. Collectively, our data offer an important resource for investigating the mechanism of nodule organogenesis and symbiotic nitrogen fixation.

**Key words:** single-cell RNA sequencing, scRNA-seq, nodule organogenesis, symbiotic nitrogen fixation, indeterminate nodule, legume plant

**Ye Q., Zhu F., Sun F., Wang T.-C., Wu J., Liu P., Shen C., Dong J., and Wang T.** (2022). Differentiation trajectories and biofunctions of symbiotic and un-symbiotic fate cells in root nodules of *Medicago truncatula*. Mol. Plant. **15**, 1852–1867.

## INTRODUCTION

Root nodules are the symbiotic organs of legumes that perform atmospheric nitrogen fixation with rhizobia. They can be classified as indeterminate nodules (such as those of *Medicago truncatula* or *Pisum sativum*) and determinate nodules (such as those of soybean and *Lotus japonicus*) by with or without the persistent apical meristem (Sprent, 2007; Stacey, 2007; Roy et al., 2020). The apical meristem of indeterminate nodules has the capability to develop into continuous differentiated zones, which results in a cylindrical shape with a much more complicated structure and more subdivided cellular function in this nodule type. The central tissue in indeterminate nodules has been classified into five zones, generally the meristematic zone (ZI), infection zone (ZII), interzone (IZ), fixation zone (ZIII), and senescence zone (ZIV) (Vasse et al., 1990), whereas the cells inside each zone are not identical (Limpens et al., 2013; Roux et al., 2014). Aside from the central part, specific studies on peripheral tissues,

such as the nodule parenchyma and vascular tissues, are quite limited. These tissues are similar to the production lines in a factory, with different divisions of work but also interconnected. However, the interaction between different tissues in nodules lacks systematic analysis.

The transcriptome patterns of symbiosis-associated genes are important for nodule organogenesis and effective nitrogen fixation. To consider the time dimension, a number of transcriptome profiles of roots and nodules from hours to days post rhizobia inoculation in the model plant, *M. truncatula*, were determined to analyze the dynamic changes in genes during nodulation (El Yahyaoui et al., 2004; Tesfaye et al., 2006; Larainzar et al., 2015; Schiessl et al., 2019). From a spatial perspective,

previous studies decomposed the central part of nodules in *M. truncatula* by laser-capture microdissection (LCM) and conducted transcriptome analysis based on Affymetrix Medicago GeneChips or RNA sequencing (RNA-seq) at a subtissue resolution (Limpens et al., 2013; Roux et al., 2014). However, there has been no further panoramic analysis of root nodules at a cellular resolution, answering how the nodule cells are organized and differentiated to execute their delicate biological functions.

Single-cell RNA-seq (scRNA-seq) technology has the great advantage of high resolution to resolve transcriptome patterns within highly heterogeneous tissues (Kolodziejczyk et al., 2015; Shaw et al., 2021). Several single-cell resolution profiles of plant roots, shoot apex, and leaves have been reported in recent years (Denyer et al., 2019; Jean-Baptiste et al., 2019; Ryu et al., 2019; Zhang et al., 2019, 2021a, 2021b; Liu et al., 2020, 2021). It is promising but also challenging to apply this technology to legume root nodules. The most difficult part is the experimental operation, especially quick and sufficient nodule protoplast isolation and purification. Although an efficient method was reported previously for root protoplast isolation in *M. truncatula* and *L. japonicus*, it took 8–12 h for cell wall digestion (Jia et al., 2018), not to mention the more complex nodules. The long protoplast purification process could affect the cell state and RNA quality for next-step sequencing (Shaw et al., 2021).

To better understand how legume plants form root nodules for symbiotic nitrogen fixation, we designed an optimized protocol for nodule protoplast preparation and conducted a scRNA-seq assay on 14-dpi (days post inoculation) nodules of *M. truncatula*. We classified 13 nodule cell clusters and analyzed their distinct expression characteristics and spatial distribution. We also uncovered differentiation trajectories of symbiotic and un-symbiotic fate cells by algorithm and analyzed their basic biofunctions. Furthermore, we discovered that the synthesis, metabolism, and transportation of a large number of nutrients as well as signaling and defense substances have different cellular distributions. These results provide considerable resources and novel insights into nodule organogenesis and symbiotic nitrogen fixation in legumes at a single-cell resolution.

## RESULTS

### Nodule protoplast preparation and scRNA-seq

To analyze the panoramic expression patterns of nodule cells, we selected the 14-dpi nodules as the research object, which usually have the meristematic zone (ZI), infection zone (ZII), interzone (IZ), and nitrogen fixation zone (ZIII), and have a continuously enhanced nitrogen fixation capacity (Figure 1D). We first designed a modified experimental procedure for nodule protoplast preparation (Figure 1A; Supplemental Figure 1). For the first-step protoplast isolation, we improved the enzyme system for cell wall digestion and combined it with the mechanical method to aid in nodule protoplast release, which reduced the enzymatic hydrolysis time to 2.5 h (Supplemental Figure 1A). The isolated protoplast includes infected cells (diameter 30–50  $\mu\text{m}$ ) and un-infected cells (diameter 5–10  $\mu\text{m}$ ). Given the huge differences in cell volume and organelles between the nodule cells infected or not infected by rhizobia (Selker and Newcomb, 1985), the second-step protoplast purification should be performed separately to avoid cell

rupture during centrifugation. The infected cells were collected by the natural sinking method, while the un-infected cells were collected by the sucrose flotation method (Supplemental Figure 1B). The purified protoplasts were then mixed together for cell counting, 10X Genomics library preparation and sequencing (Supplemental Figure 1C).

Two independent replications were performed, and over 18 000 cells from the 2 samples (A17\_NOD1 and A17\_NOD2) were loaded into the 10X Genomics scRNA-seq platform. After data filtration at both the cell and gene levels, we obtained the expression data of 22 228 genes (42% of the total annotated genes in the *Medicago* genome) in a total of 9756 cells (Supplemental Figure 2; Supplemental Table 1). By linear dimensional reduction based on principal-component analysis (PCA), these nodule cells could be clustered differently at different resolutions (Figure 1B). At a resolution of 0.1, the cells were divided into six major clusters and, as the resolution increased, so did the number of clusters. Considering the known distinguished nodule tissues/zones (Xiao et al., 2014), we chose a moderate resolution of 0.4 for further analysis, which led to the classification of 13 cell clusters (Supplemental Table 2). The 13 clusters were visualized by *t*-distributed stochastic neighborhood embedding (*t*-SNE) (Supplemental Figure 3A) and Uniform Manifold Approximation and Projection (UMAP) (Figure 1C), and the data from the two independent samples showed good repeatability (Supplemental Figure 3B). We retrieved the expression data of the top 20 marker genes from each cluster in all 9756 cells for heatmap analysis and found that these marker genes were enriched in the cluster they represented, except cluster 0 (Supplemental Figure 4). Therefore, we identified 13 cell clusters with distinct expression characteristics in 14-dpi nodules by scRNA-seq.

### Nomenclature of cell clusters in indeterminate nodules

To preliminarily distinguish and annotate the 13 cell clusters, we referred to reported symbiosis-related genes (Figure 2A; Supplemental Table 3). We found that the reported meristem-expressed marker genes *ANNEXIN 1* (*MtANN1*) (Niebel Fde et al., 1998), *SHORT HYPOCOTYL2* (*MtSHY2*)/*IAA3* (Limpens et al., 2013; Roux et al., 2014), *PLETHORA 3* (*MtPLT3*) (Franssen et al., 2015) and its homologous gene *MtPLT5*, along with the cell-cycle-associated genes *CYCLIN-DEPENDENT KINASE 2* (*MtCDK2*) and *MtCDKB2;2* (Limpens et al., 2013; Roux et al., 2014) were specifically enriched in cluster 7, and the nodule apex specific genes *NODULIN 13* (*MtN13*) (Gamas et al., 1996, 1998) and *MtPLT4/MtBBM* (Franssen et al., 2015) were specifically expressed in cluster 5. Thus, clusters 5 and 7 were annotated as Nodule Apex1 (NA1) and Nodule Apex 2 (NA2). The nod factor receptor *LysM DOMAIN RECEPTOR-LIKE KINASE 3* (*MtLYK3*) (Limpens et al., 2005) was detected with higher expression in both clusters 4 and 7, and the infection zone-enriched genes *MtN2* (Gamas et al., 1996) and *EARLY NODULIN 11* (*MtENOD11*) (Journet et al., 2001), along with *ERF REQUIRED FOR NODULATION 1* (*MtERN1*) (Cerri et al., 2012; Liu et al., 2019), were enriched in cluster 4. Another marker gene, *MtN6*, which was observed ahead of growing infection threads and in the pathway involved in preparation for infection (Mathis et al., 1999), was also specifically expressed in cluster 4. Therefore, we inferred cluster 4 to be Pre-infected

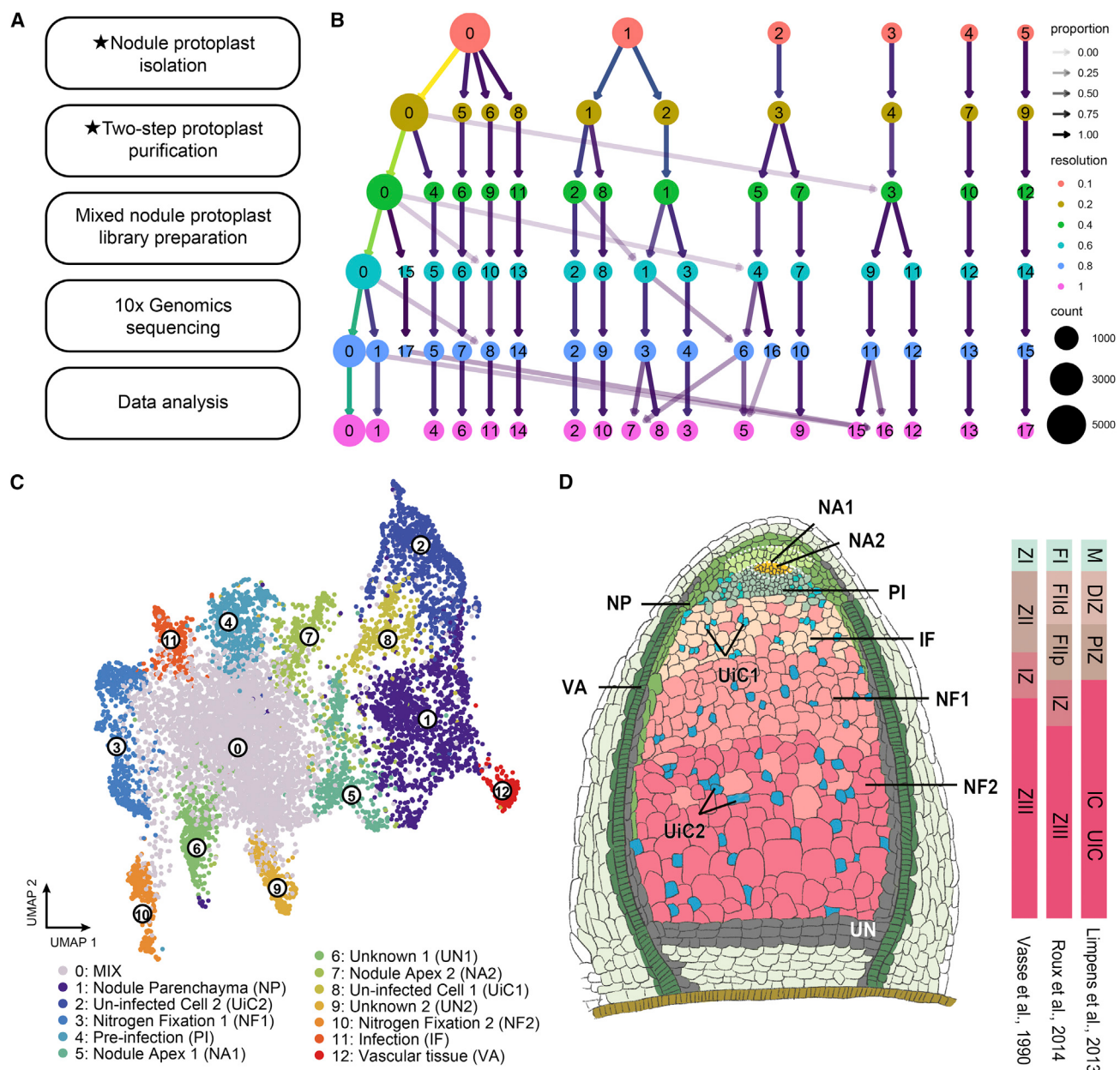


**Figure 1. Cell clustering in mature nodules of *Medicago truncatula*.**

(A) Flow chart of scRNA-seq of root nodules. Stars signify the improved experimental procedures.

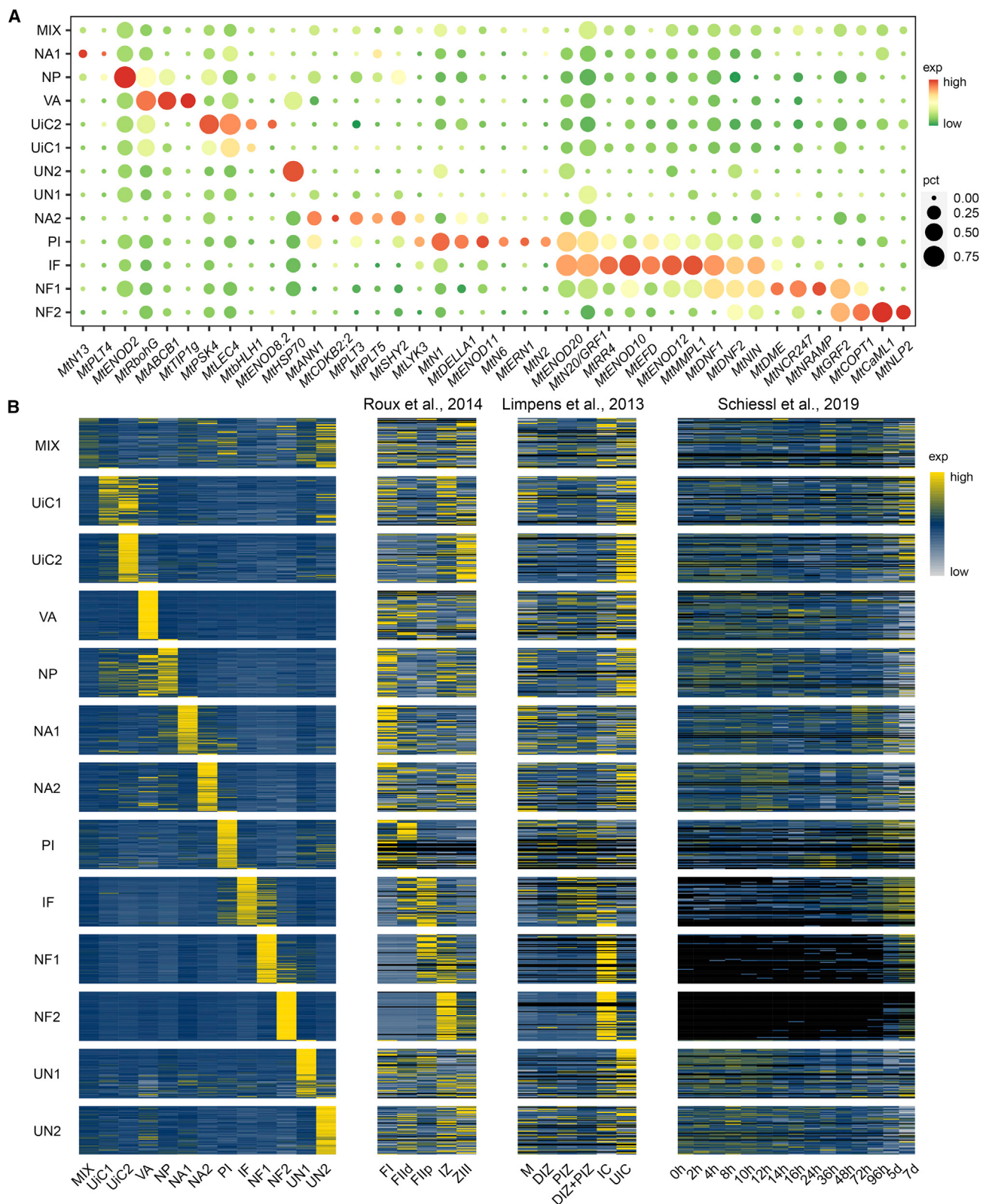
(B) Clutree showing clustering under different resolutions set in Seurat. Circle size, cell number; circle color, resolution; arrow transparency, proportion in the cluster.

(C) Thirteen cell clusters displayed by UMAP. Dots, individual cells.  $n = 9756$  cells.

(D) Sketch of the longitudinal section of an indeterminate nodule with classic partition and cell type annotations. ZI, meristematic zone; ZII, infection zone; IZ, interzone; ZIII, nitrogen fixation zone (Vasse et al., 1990). FI, meristematic zone; FII, distal infection zone; FIIp, proximal infection zone; IZ, interzone; FIII, nitrogen fixation zone (Roux et al., 2014). M, meristematic zone; DIZ, distal infection zone; PIZ, proximal infection zone; IC, infected cells from nitrogen fixation zone; UIC, un-infected cells from nitrogen fixation zone (Limpens et al., 2013).

(PI). As *MtN20/GROWTH-REGULATING FACTOR 1* (*MtGRF1*) (Maia, 2018) was highly expressed in clusters 4 and 11 and the infection zone-enriched *ENOD12* (Pichon et al., 1992), *ERF REQUIRED FOR NODULE DIFFERENTIATION* (*MtEFD*) (Vernie et al., 2008; Saur et al., 2011), and *MtN9/MATRIX METALLOENDOPROTEINASE-LIKE1* (*MtMMPL1*) (Combier et al., 2007) were specifically expressed in cluster 11, it was termed Infection (IF). The signal peptidase complex subunit

*DEFECTIVE IN NITROGEN FIXATION 1* (*MtDNF1*) (Wang et al., 2010) was expressed in clusters 11 and 3, and the bacteroid differentiation-associated *NODULE-SPECIFIC CYSTEINE-RICH 247* (*MtNCR247*) (Farkas et al., 2014), the interzone-specific *DEMETER* (*MtDME*) (Satgé et al., 2016), and some leghemoglobins, such as *MtLb3* and *MtLb9*, were specifically expressed in cluster 3; thus, cluster 3 was defined as Nitrogen Fixation 1 (NF1). The symbiosome membrane-localized *COPPER*

**Figure 2. Typical expression characteristics of each nodule cell cluster.**

(A) Expression patterns of the reported marker genes in each cluster. Dot color, relative expression level; dot size, percentage of cells expressing the marker gene.

(B) Heatmap showing the expression patterns of the top 50 marker genes in each cluster from different transcriptome data (Limpens et al., 2013; Roux et al., 2014; Schiessl et al., 2019). Color bar, relative expression level ("N/A" is shown in black).

*TRANSPORTER 1 (MtCOPT1)* (Senovilla et al., 2018) was highly expressed in clusters 3 and 10, and another symbiosome-localized *CALMODULIN-LIKE 1 (MtCAML1)* (Liu et al., 2006) was also enriched in cluster 10. In addition, the majority of symbiotic leghemoglobins (Ott et al., 2005) showed higher expression levels in cluster 10 (Supplemental Figure 5; Supplemental Table 4). Therefore, we defined cluster 10 as Nitrogen Fixation 2 (NF2). The conserved nodule parenchyma specific *MtENOD2* (van de Wiel et al., 1990; Allen et al., 1991) was enriched in cluster 1; thus, we designated cluster 1 as Nodule Parenchyma (NP). As the vascular tissue-specific *RESPIRATORY BURST OXIDASE HOMOLOGUE G (MtRboHg)* (Marino et al., 2011) was highly expressed in cluster 12, we considered cluster 12 as Vascular tissue (VA). We found that *M. truncatula BASIC HELIX-LOOP-HELIX 1 (MtbHLH1)*, which was reported to be expressed in the un-infected cells inside the nitrogen fixation zone (Godiard et al., 2011), was specifically detected in cluster 2, and nodule-specific *LECTIN 4 (MtLEC4)*, a homolog to *MtLEC1*, *MtLEC2*, and *MtLEC3*, which were proven to be highly expressed in the un-infected cells inside both the infection zone and nitrogen fixation zone (Bauchrowitz et al., 1996), was enriched in clusters 2 and 8 in our data. Thus, we designated clusters 8 and 2 as Un-infected Cell 1 (UiC1) and Un-infected Cell 2 (UiC2), respectively. For clusters 6 and 9, there were few reported specific marker genes; thus, these clusters were defined as Unknown 1 (UN1) and Unknown 2 (UN2), respectively. In addition, considering that cluster 0 lacks typical expression patterns of any marker genes, we defined it as MIX.

To further understand the properties of these cell clusters, we compared the scRNA-seq data with the published transcriptome data based on LCM (Figure 2B; Supplemental Table 5). We selected the top 50 marker genes from each cluster and screened their expression data in different tissues/zones of 15-dpi nodules (Roux et al., 2014) and 21-dpi nodules (Limpens et al., 2013). Compared with the results of Roux et al. (2014), a great portion of the marker genes of NA1, NA2, and NP were enriched in the meristematic zone (FI); the marker genes of PI, IF, NF1, and NF2 were subsequently enriched in the distal infection zone (FIId), proximal infection zone (FIIp), and interzone (IZ); and the marker genes of UiC2 were quite enriched in the nitrogen fixation zone (FIII). On the other hand, compared with Limpens et al. (2013), the marker genes of NF1 and NF2 were enriched in infected cells from the fixation zone, while those of UiC1 and UiC2 were enriched in un-infected cells localized in the fixation zone. We also retrieved the expression data from Schiessl et al. (2019) to investigate the expression changes of the marker genes in the early stage of nodulation, and found that a large proportion of the marker genes of NF1 and NF2 were almost undetectable from 0 to 96 h, but upregulated from 5 to 7 days, which indicates their function along with the appearance of the nitrogen fixation zone. Furthermore, the marker genes of PI and IF were also upregulated post inoculation, and the time point of upregulation seemed earlier than that of NF1 and NF2. The consistency of these data indicates that our annotation of the cell clusters is quite appropriate. For a clearer description and analysis, we refer to the cell clusters that are about to or have already been infected by rhizobia as the symbiotic fate group (PI, IF, NF1, and NF2), and that would not be infected as the un-symbiotic fate group (NP, UiC1, UiC2, and VA).

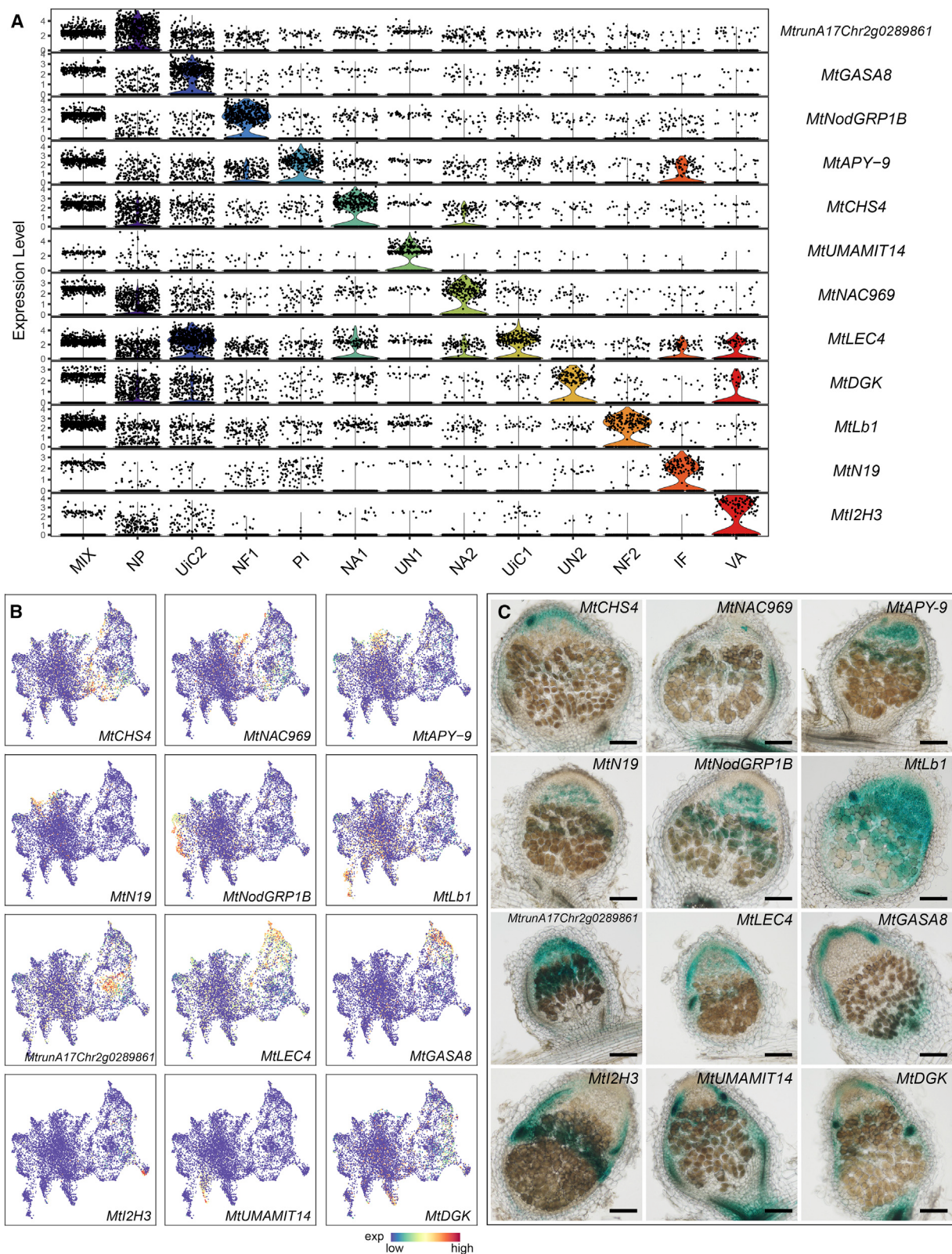
### Construction of a physical cellular map of indeterminate nodules

To further investigate the spatial distribution of these cell clusters, we screened the specific marker genes for each cell cluster from perspectives of considering both the expression level and ratio (Figure 3A and 3B; Supplemental Table 6) and verified their tissue localization experimentally (Figure 3C). The expression data of these genes from Roux et al. (2014), Limpens et al. (2013), and Schiessl et al. (2019) were retrieved to help identify their expression patterns in terms of time and space (Supplemental Figure 6). We utilized the promoter-GUS fusion system mediated by hairy root transformation and collected and stained the roots and nodules at 21 dpi, when the nodules on the transformants were mature and able to fix nitrogen. The GUS staining assay showed that the transformants of *MtCHS4*, which was specifically expressed in NA1, had  $\beta$ -glucuronidase activity on the distal end of the nodule, which was limited to a few cell layers; while the transformants of *MtNAC969*, which was enriched in NA2, showed staining in a very small group of cells at the meristem (Figure 3C). Along the central axis of the nodule, the staining signals in the transformants of *MtAPY-9*, *MtN19*, *MtNodGRP1B*, and *MtLb1* showed successive developmental stages of PI, IF, NF1, and NF2, respectively (Figure 3C). The transformants of *MtrunA17Chr2g0289861*, which was specifically expressed in NP and annotated as an unknown gene, showed a peripheral staining pattern, while the VA marker, *MtI2H3*, showed expression patterns along the vascular tissues (Figure 3C). *MtLEC4* was enriched in both UiC1 and UiC2, and staining of the transformants of *MtLEC4* was observed in the central and peripheral tissues of the meristem, infection zone, and interzone (Figure 3C). The UiC2 marker *MtGASA8*, which was also expressed at a moderate level in NP and UiC1 cells, showed staining in the un-infected cells inside the nitrogen fixation zone and around the endothelial layer (Figure 3C). The UN1 marker, *MtUMAMIT14*, showed expression patterns surrounding the nodule central tissue, while the UN2 marker, *MtDGK*, which was also expressed in VA, NP, and UiC2, showed similar spatial characteristics to UN1 (Figure 3C). This result indicates that the two unknown cell clusters are distributed in the peripheral tissues and may be subclasses of cortical or vascular bundle-associated cells.

Combining our staining results with the reported literature, we defined a refined spatial structure of the indeterminate nodule (Figure 1D). The central tissue includes meristematic cells (NA1 and NA2) and symbiotic fate cells (PI, IF, NF1, and NF2) from the distal side to the proximal side, with some un-symbiotic fate cells (UiC1 and UiC2) embedded. The peripheral tissue is usually un-symbiotic fate cells, especially NP, with a few bundles of VA surrounding the central tissue. These cell clusters are spatially mosaic and interconnected, not uniform, independent masses.

### Successive differentiation trajectory reconstruction of symbiotic and un-symbiotic cells

To further understand how different nodule cell clusters are organized and interconnected, we performed pseudotime analysis. As UMAP can provide the meaningful organization pattern of cell clusters, and the two meristematic cell clusters (NA1 and NA2) localized between the symbiotic fate cells (PI, IF, NF1,

**Figure 3. Physical distribution of each cluster represented by specific marker genes.**

(A) Violin plots showing the expression levels of the specific representative genes. Dots, individual cells.

(B) UMAP showing the expression distribution of the specific representative genes. Dots, individual cells; color bar, relative expression level.

(C) GUS staining assay showing the expression patterns of the specific representative genes in 21-dpi nodules from transgenic hairy roots. Scale bar corresponds to 100  $\mu$ m.

and NF2) and the un-symbiotic fate cells (NP, UIC1, UIC2, and VA) (Figure 1C), we assumed these two clusters to be developmental initiation. It is also quite clear that NA1 was adjacent to the un-symbiotic cells, while NA2 was closer to the symbiotic cells. This finding indicates that the two kinds of apex meristem cells in indeterminate nodules have distinct expression patterns and differentiate into differing cell populations.

We adopted the Monocle 2 method to reconstruct the differentiation trajectories of the symbiotic and un-symbiotic cell groups and visualized them by DDRTree (Figure 4A and 4D) (Qiu et al., 2017). We extracted NA2, PI, IF, and NF1 for analysis of the symbiotic group and specified NA2 as the beginning of pseudotime. The four cell clusters could be classified into three states, with NA2 and PI as the first state, PI and IF as the second state, and IF and NF1 as the third state. The differentiation trajectory of these clusters is consistent with the well-known successive developmental process of the symbiotic components in the indeterminate nodule (Figure 4A). We selected the top 50 differentially expressed genes (DEGs) from each cluster for heatmap analysis, and found that their expression patterns were consistent with the presumed differentiation trajectory along the pseudotime (Figure 4B; Supplemental Table 7). We were particularly concerned that many *ODULE-SPECIFIC CYSTEINE-RICH PEPTIDE* (NCR) and *ODULE-SPECIFIC GLYCINE-RICH PEPTIDE* (NodGRP) genes, which have potential antimicrobial activity (Alunni et al., 2007), were enriched in PI, IF, and NF1. NCR peptides are known to act in host-rhizobia specificity and orchestrate the terminal differentiation of bacteroids (de Bang et al., 2017). There were subtle temporal differences between their expression (Figure 4C), implying complex regulatory networks and distinct functions.

For un-symbiotic fate cells, we extracted NA1, NP, UIC1, UIC2, and VA for further analysis, and NA1 was designated developmental initiation. The DDRTree showed a complex distribution pattern in this group. Specifically, NA1, UIC2, and VA showed distribution bias, especially at the end of each branch, while NP was fairly evenly distributed on each branch (Figure 4D). UIC1 showed a similar pattern to NP, but with fewer cells. This result suggests that UIC2 and VA may be more differentiated than NP and UIC1, which is consistent with their spatial distribution in which UIC1 and UIC2 are deep in the central tissue of the nodule, VA is located at the peripheral layer, and NP serves as the connection (Figure 1D). The top 50 DEGs from NA1, NP, UIC1, UIC2, and VA were clustered into four groups. Groups 2, 3, and 4 were enriched in DEGs of NA1, UIC2, and VA, respectively, while group 1 was enriched in DEGs of NP and UIC1 (Figure 4E; Supplemental Table 8). We further focused on the expression patterns of the DEGs along the pseudotime and observed that their distribution was consistent with the developmental trajectory (Figure 4F).

For further verification, we adopted Monocle 3, which has algorithm upgrades in learning the principal graph (Cao et al., 2019). In the Monocle 3 analysis, all 13 cell clusters were taken into account systematically, and the developmental trajectory could be presented in the form of UMAP. We selected NA1 and NA2 as the roots and found that the trajectory extended from the middle to both sides, and that NF1, NF2, UN1, UIC2, and

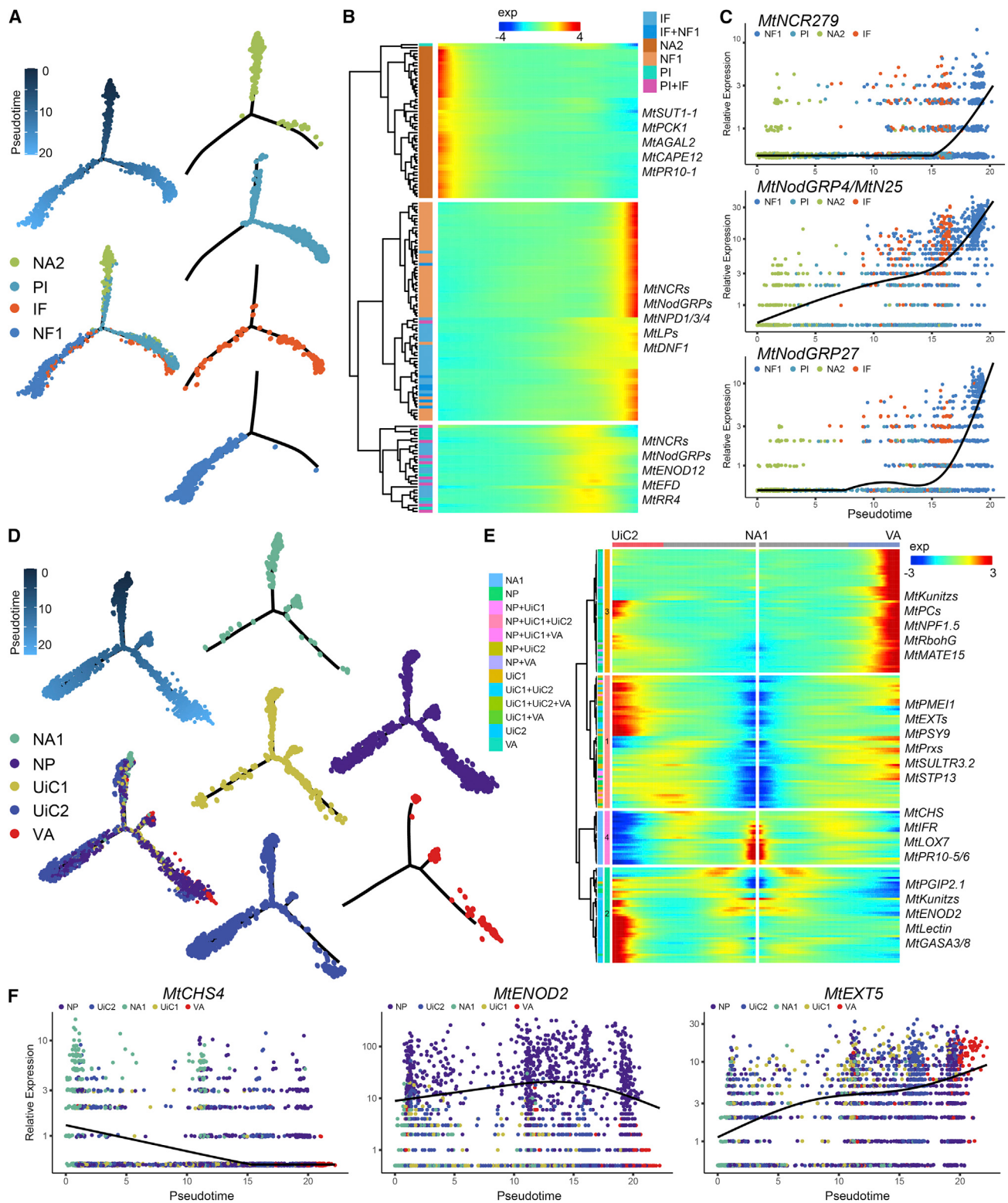
VA had relatively high degrees of differentiation (Supplemental Figure 7). The divergent developmental trajectories of the symbiotic and un-symbiotic cells were consistent with the results of the Monocle 2 analysis.

### Basic biological function analysis of each cell cluster

To further understand the overall functions of the 13 cell clusters, we selected the top 100 marker genes from each cell cluster for gene ontology (GO) enrichment analysis, especially for biological processes (Supplemental Figure 8). For meristematic cells, a large portion of NA1 marker genes are involved in flavonoid biosynthesis, which plays an important role as signaling molecules in nodule development, while NA2 is more engaged in branched-chain amino acid (AA) catabolic processes. Among the symbiotic fate cells, the GO term “nodulation,” which refers to nodule development, is enriched in both PI and IF; PI is also related to the sterol biosynthetic process, and IF is involved in signal peptide processing and cell wall biogenesis. For the nitrogen fixation cells, the GO term “oxygen transport” is enriched in NF2, which is significant for the energy demands of symbionts (Jiang et al., 2021). Nevertheless, since a great proportion of the marker genes in NF1 lack annotations, few GO terms were enriched in this cluster (Supplemental Table 9). For un-symbiotic fate cells, NP, UIC2, and VA are involved in cell wall biogenesis, which might affect the expansion of cells, allowing for the whole nodule to enlarge, and NP also has an active role in the cellular redox reaction, which corresponds to its distribution as an outer layer of the central symbiotic tissue. As part of the vascular-associated system, NP and VA participate in the transportation of various metabolites. Interestingly, the GO term “glutamine metabolic process” is enriched in UIC2, which suggests an important function of the un-symbiotic fate cells in nitrogen assimilation. For the unknown cell clusters, although there were no reported marker genes with explicit functional analysis, the GO assay results suggest that UN2 is actively involved in protein processing and folding, particularly under stress conditions, while UN1 may be related to the redox state of the organ. Combined with their physical distribution, we supposed that the unknown cells belong to the un-symbiotic group and could be subsets of cortical or vascular cells.

### The synthesis and metabolism of different flavonoids are finely regionalized in symbiotic and un-symbiotic cells

Flavonoids play various key roles during nodulation. For example, they serve as inducers of nod factor synthesis in rhizobia, regulate host specificity, and inhibit auxin transportation, resulting in auxin accumulation at the initial stage of nodule organogenesis (Buer et al., 2010; Liu and Murray, 2016; Gifford et al., 2018). According to the GO enrichment assay, 20.83% (20/96) of the top 100 marker genes in NA1 were annotated with “flavonoid biosynthetic process,” and 10.42% (10/96) were annotated with “chalcone biosynthetic process,” which aroused our interest (Supplemental Figure 8; Supplemental Table 9). We searched for the expression data of the key enzymes in the phenylpropane metabolic pathway and the legume-specific isoflavone metabolic pathway, and found that a number of them were enriched in NA1, NP, and VA (Figure 5A and 5B; Supplemental Table 10; Supplemental Figure 9). Consistent with that, most of these genes were also relatively highly expressed in the meristematic zone (Fl) from the

**Figure 4. Differentiation trajectories of symbiotic or un-symbiotic fate cells.**

(A and D) DDRTree showing the differentiation trajectories of symbiotic fate cells (NA2, PI, IF, NF1) (A) or un-symbiotic fate cells (NA1, NP, UiC1, UiC2, VA) (D) along pseudotime. Dots, individual cells;  $n = 1706$  for symbiotic fate cells;  $n = 3102$  for un-symbiotic fate cells.

(B and E) Heatmap showing hierarchical clustering of the expression of the top 50 DEGs in each symbiotic cell cluster (B) or un-symbiotic cell cluster (E) along pseudotime. Representative genes are listed on the right. Color bar, relative expression level.

(C and F) Expression of typical marker genes in symbiotic fate cells (C) or un-symbiotic fate cells (F) along pseudotime. Dots, individual cells.

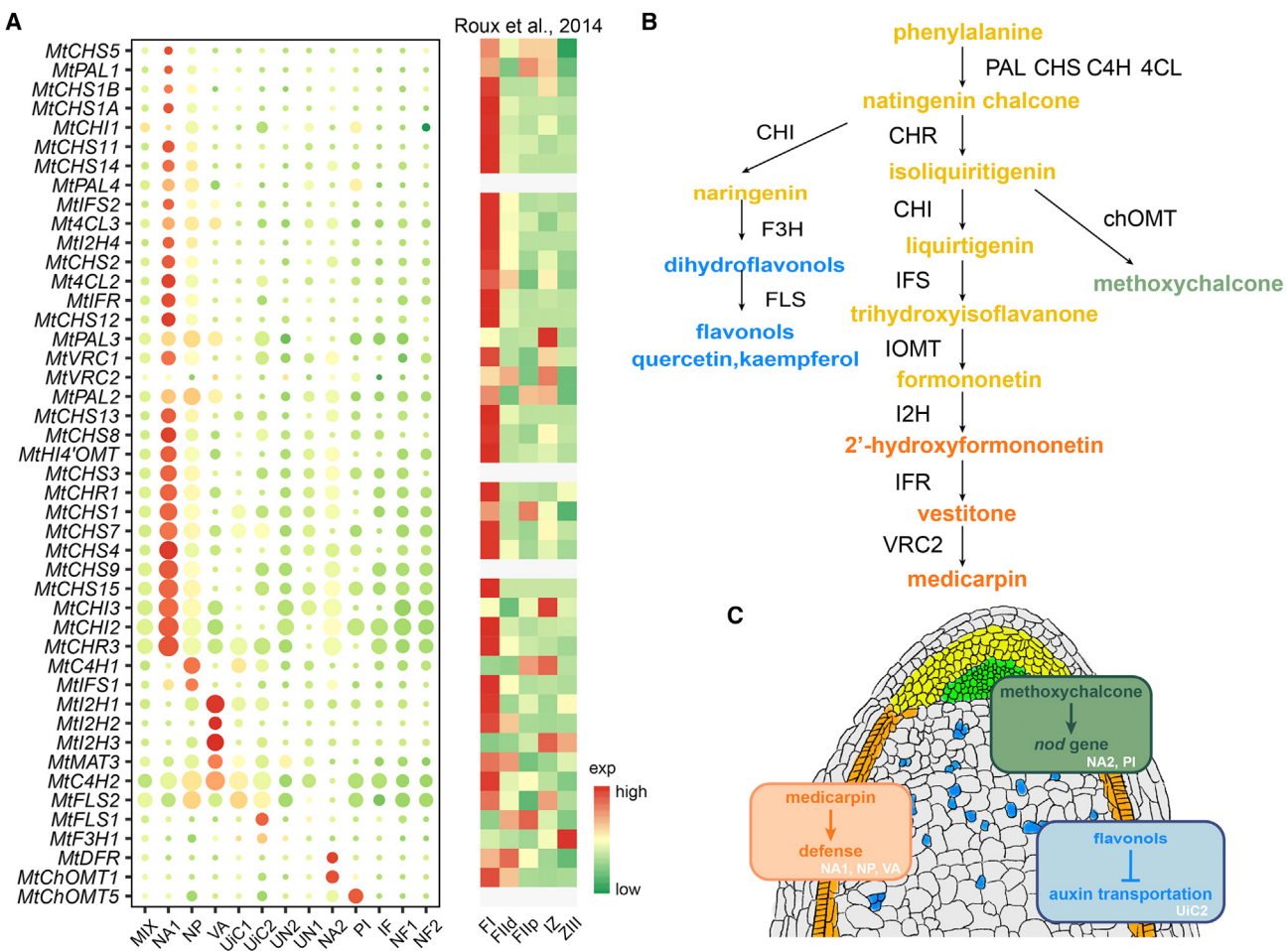


**Figure 5. Regionalization of the key enzymes in flavonoid synthesis and metabolism in nodules.**

(A) Expression patterns of the key enzymes of flavonoid synthesis and metabolism in scRNA-seq and LCM-based RNA-seq (Roux et al., 2014). Dot size, percentage of cells expressing the marker gene; color bar, relative expression level (“N/A” is shown in light gray).

(B) Scheme of the major flavonoid synthesis and metabolism pathways in nodules. Enzymes shown in black. Colors of flavonoids correspond to their main synthesized place. NA1 is shown in yellow; NP and VA are shown in orange; NA2 is shown in green; UIC2 is shown in blue. Arrows showing the synthesis direction.

(C) Model of the hypothetical distribution of major flavonoids in nodules. The *nod* gene inducer methoxychalcone is synthesized in NA2 and PI. The *nod* gene antagonism factor medicarpin and its upstream flavonoids are synthesized in NA1, NP, and VA. The auxin transportation inhibitor flavonols are synthesized in UIC2.

LCM-based transcriptome data of the 15-dpi nodules (Roux et al., 2014). Among these genes, the majority were expressed in NA1 and NP, such as PHENYLALANINE AMMONIA LYASE (*MtPAL*), CINNAMIC ACID 4-HYDROXYLASE (*MtC4H*), 4-COUMARATE COA LIGASE (*Mt4CL*), CHALCONE SYNTHASE (*MtCHS*) CHALCONE REDUCTASE (*MtCHR*), CHALCONE ISOMERASE (*MtCHI*), and ISOFLAVONE SYNTHASE (*MtIFS*), which made up the pathway converting phenylpropane to isoflavones, and the downstream ISOFLAVONE 2'-HYDROXYLASE (*Mt12H*), ISOFLAVONE 4'-O-METHYLTRANSFERASE (*Mthi4'OMT*), and VESTITONE REDUCTASE CLUSTER 2 (*MtVRC2*), which led to the final product of the phytoalexin, medicarpin, possibly antagonizing *nod* gene expression as well as inhibiting the invasion of pathogens (Zuanazzi et al., 1998; Guenoune et al., 2001). Conversely, we also found that two CHALCONE O-METHYLTRANSFERASES (*MtChOMTs*) were enriched in NA2 and PI (Figure 5A), which may differentiate into infected cells. *ChOMTs* encode the key enzyme for the biosynthesis of methoxychalcone, which is identified as a

stronger inducer of the *nod* gene, even over luteolin (Maxwell et al., 1989). In addition, FLAVANONE 3-HYDROXYLASE (*MtF3H*) and FLAVONOL SYNTHASE (*MtFLS*), which contribute to flavonol biosynthesis were enriched in UIC2 (Figure 5A), and their catalytic products have been reported to inhibit auxin transportation downstream of cytokinin signaling (Silva-Navas et al., 2016). Therefore, these results indicate that the biosynthesis of differing flavonoids are finely regulated in different cell clusters of the thriving nodules (Figure 5C), and that their distribution features may supervise the infected or un-infected cell groups during symbiosis.

#### Un-infected cell 2 is the main site for asparagine synthesis

The core biofunction of root nodules is to convert atmospheric nitrogen to ammonia for further utilization, and AA biosynthesis and transportation processes are important components of the whole

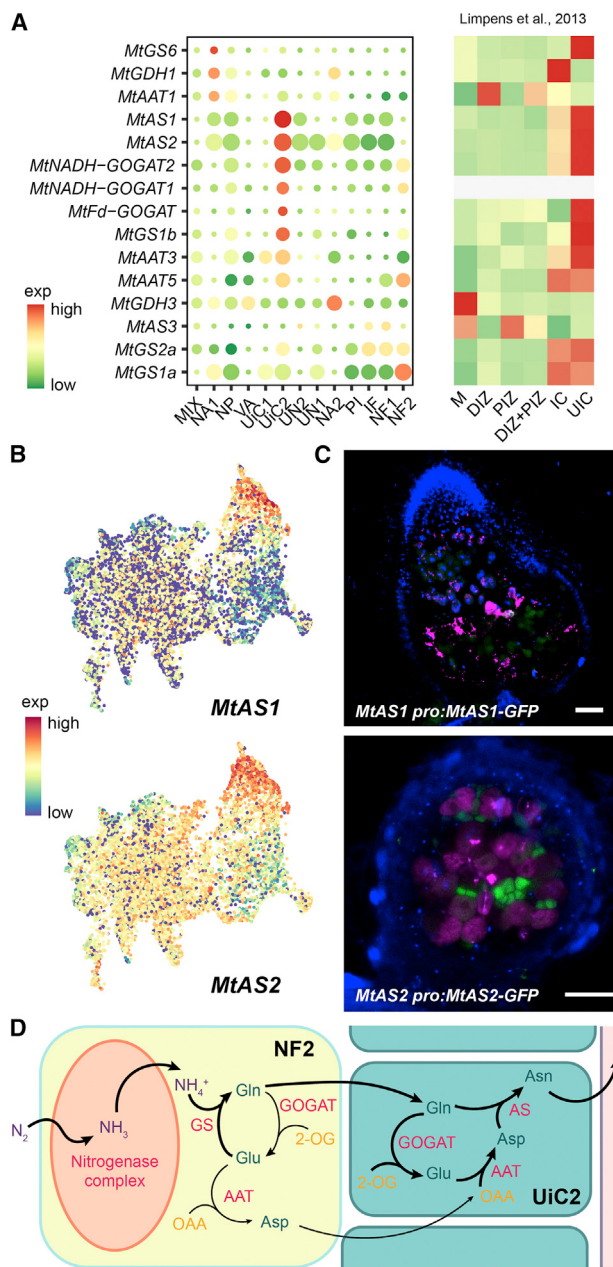


**Figure 6.** UIC2 and NF2 coordinate nitrogen assimilation.

(A) Expression patterns of the key enzymes of nitrogen assimilation in scRNA-seq and LCM-based RNA-seq (Limpens et al., 2013). Dot size, percentage of cells expressing the marker gene; color bar, relative expression level ("N/A" is shown in light gray).

(B) UMAP showing the expression distribution of *MtAS1* and *MtAS2*. Dots, individual cells; color bar, relative expression level.

(C) Expression patterns of *MtAS1 pro:MtAS1-GFP* and *MtAS2 pro:MtAS2-GFP* in 28-dpi nodules from transgenic hairy roots inoculated with RFP-tagged rhizobium. GFP is shown in green; RFP is shown in pink; DAPI is shown in blue. Scale bar corresponds to 100  $\mu$ m.

(D) Scheme of the nitrogen assimilation pathway in the nitrogen fixation zone. Nitrogen and its primary assimilation products in the symbiosomes of nitrogen fixation cells are marked in purple. Amino acid products are marked in blue. Basic organics providing carbon skeletons are marked in orange. Enzymes are marked in pink.

production line. It is well known that nitrogenase catalyzes the first step of nitrogen fixation in bacteroids, and the converted  $\text{NH}_4^+$  is assimilated by the glutamine synthetase (GS)/glutamate synthase (GOGAT) cycle into glutamine (Gln) and glutamate (Glu) (Temple et al., 1998; Forde and Lea, 2007). We identified that *MtGS1a* and *MtGS2a* were mainly expressed in NF2 (Figure 6A; Supplemental Table 11), and *MtGS1a* was previously proven to account for 90% of GS activity during nodulation (Carvalho et al., 2003). However, we also found that plastid-localized *MtFd-GOGAT* was specifically expressed in UIC2, and that *MtGS1b* and cytoplasmic *MtNADH-GOGAT1/2* were enriched in both UIC2 and NF2, the expression levels of which were even higher in UIC2 (Figure 6A; Supplemental Table 11). These results indicate that Gln is the major nitrogen assimilation product in NF2, while Glu is synthesized more in UIC2 (Figure 6D).

Asn is the major AA in nodules, and serves as the main nitrogen transport compound in *Medicago* (Ta et al., 1986). Intriguingly, we found that nodule-expressed asparagine synthetases (ASs), which transfer the  $-\text{NH}_2$  group from Gln to Asn, were highly expressed in UIC2 (Figure 6A and 6B; Supplemental Table 11). To further confirm the expression patterns, we constructed the transgenic hairy roots with *MtAS1 pro:MtAS1-GFP* and *MtAS2 pro:MtAS2-GFP* cassettes. The transformants were inoculated with Sm1021-RFP and detected at 28 dpi. We observed the specific fluorescent signals of GFP fusion proteins from the uninfected cells in the nitrogen fixation zone (Figure 6C). In the LCM-based transcriptome data provided in Roux et al. (2014) and Limpens et al. (2013), *MtAS1* and *MtAS2* were also specifically expressed in nitrogen fixation zones, especially the un-infected cells (Figure 6A; Supplemental Figure 10). This result suggests that the Asn synthesis pathway is assigned to the un-infected cells located around the nitrogen fixation cells containing symbiosomes (Figure 6D). Hence, these results indicated that  $\text{NH}_4^+$  is assimilated into Gln in NF2, while UIC2 is the main workplace for Asn synthesis.

#### Cell-type-dependent loading and transportation of synthesized AAs in nodules

AA metabolism is tightly coordinated with its transportation process (Dinkeloo et al., 2018). Nevertheless, how nodule-synthesized AAs, such as Gln and Asn, are transported across these tissues for further utilization in other parts of the plant is significant but largely unknown in *M. truncatula*. The synthesized AAs need to be exported into the apoplast across membranes from NF2 and UIC2 and uploaded to the peripheral tissues and then into vascular bundles for long-distance transportation to the aboveground part. Hence, we screened all the candidate AA transporters from our data (Figure 7A and 7B; Supplemental Table 12). We found that several nodule-enriched AA transporter genes were specifically expressed in IF and NF1, such as CATIONIC AMINO ACID TRANSPORTER 1 (*MtCAT1*) (Yang et al., 2014), AMINO ACID PERMEASE 30 (*MtAAP30*), and LYSINE AND HISTIDINE TRANSPORTERS 10 (*MtLHT10*), which are capable of importing AAs (Rentsch et al., 2007; Tegeder and Ward, 2012). Thus, we speculated that these transporters play important roles in branched-chain AA supplementation for rhizobia differentiation (Figure 7C). There were also a few USUALLY MULTIPLE ACIDS MOVE IN AND OUT

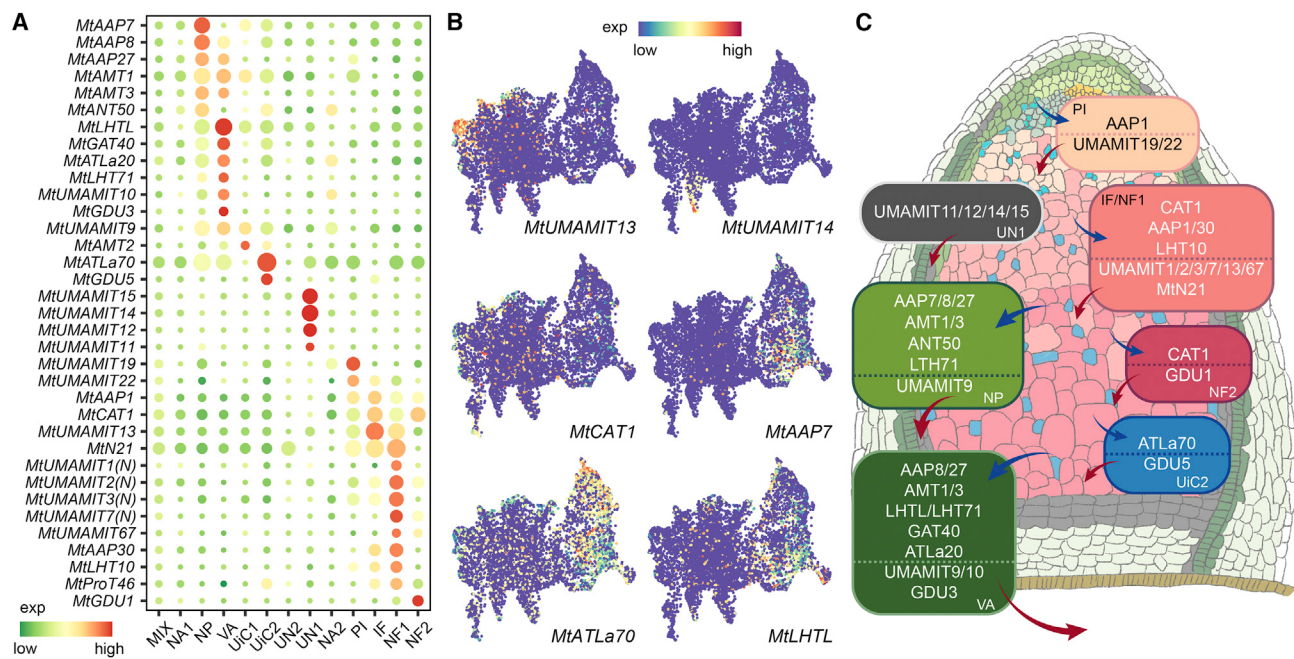


**Figure 7. Network of amino acid transportation in nodules.**

(A) Expression patterns of the putative amino acid transporters in nodules and key enzymes in flavonoid synthesis and metabolism pathways. Dot size, percentage of cells expressing the marker gene; color bar, relative expression level.

(B) UMAP showing the expression distribution of the putative amino acid transporters specific to differing cell clusters. Dots, individual cells; color bar, relative expression level.

(C) Model of the putative amino acid loading and transportation pathway in nodules. Blue arrows represent importation. Red arrows represent exportation.

**TRANSPORTER (UMAMIT)** family members in the symbiotic cells, which mostly participate in exporting AAs (Zhao et al., 2021). They are inferred to export nitrogen assimilation products, transferring them to the next-step processing line (Figure 7C). We also found that several AA transporter coding genes, such as *MtAAP7/27*, *AMMONIUM TRANSPORTER 1/3* (*MtAMT1/3*), and *AROMATIC AND NEUTRAL TRANSPORTER 50* (*MtANT50*), were enriched in NP, which is consistent with the loading process of the AAs from apoplast to cortex (Figure 7C). In addition, we found another group of AA transporter genes, such as *LHT-LIKE* (*MtLHTL*)/*MtLHT71*, *γ-AMINOBUTYRIC ACID TRANSPORTER 40* (*MtGAT40*), and *MtUMAMIT9/10*, with higher expression levels in VA, and these transporters may participate in AA absorption and further transportation in vascular bundles (Figure 7C). Interestingly, we found that two *GLUTAMINE DUMPER (GDU)*-coding genes, *MtGDU1/5*, were enriched in nodules. Previous studies indicated that GDU family proteins are involved in the efflux of several AAs, especially Gln and Asn (Pilot et al., 2004). In our data, *MtGDU1* was specifically expressed in NF2, and *MtGDU5* was preferentially expressed in UIC2, which indicates that *MtGDU1* and *MtGDU5* may be crucial proteins for synthesized AA exportation from NF2 and UIC2 (Figure 7C). Collectively, these results indicate a complete and orderly AA transport network in the indeterminate nodule.

## DISCUSSION

Here, we report a scRNA-seq profiling of root nodules in the model legume, *M. truncatula*, and generation of a refined spatial and functional cellular map. This high-precision transcriptome

sequencing was based on an optimized experimental technique that could be used to isolate and purify nodule protoplasts in a short time (Figure 1; Supplemental Figure 1). Abundant nodule cell types were reserved in the samples, including parenchyma cells and vascular tissues at the peripheral layer, which are important for nodule development but often overlooked. We designated 13 nodule cell clusters at a moderate resolution of 0.4, and named them based on their specific transcriptome patterns. Although more clusters could be produced at higher resolution, it would be difficult to distinguish and verify their biological functions (Figure 1B). Ten of the 13 cell clusters have the marker genes with typical functions, while UN1 and UN2 lack the reported representative. However, cluster 0 (MIX), which accounts for 41% of the total cells, has a vague expression pattern. To evaluate the effect of protoplasting in this research, we screened the homologs of protoplasting-induced genes (Birnbaum et al., 2003), and found that they were not significantly enriched in any specific cluster (Supplemental Figure 12), which indicates little bias of cell clustering influenced by protoplasting in this research.

We rebuilt the nodule model incorporating the physical distribution and functions of each cell type (Figure 1D). We found that the two groups of nodule apical meristematic cells differentiate into central symbiotic fate cells and peripheral and internal un-symbiotic fate cells. The symbiotic cells along with the embedded un-infected cells principally perform symbiotic nitrogen fixation, while the peripheral un-symbiotic cells provide physical barriers, ensure energy and matter transport, and maintain environmental homeostasis (Supplemental Figure S8). Compared with the

## Single-cell transcriptome in *Medicago* nodules

classic partitions of the central tissue, scRNA-seq revealed a finer organization of the indeterminate nodule. Specifically, NA1 and NA2 localize in the meristematic zone (ZI), PI, IF and part of NF1 localize in the infection zone (ZII), NF1 and part of NF2 localize in the interzone (IZ), and most of NF2 localizes in the fixation zone (ZIII) (Figure 1D). For the un-symbiotic group, NP accounts for a large proportion, which may serve as the connections between the more differentiated clusters. In screening novel specific marker genes, we found that although each cluster has unique characteristics at the transcriptome level, the individual marker genes did not seem to be adequately representative (Figure 3C). The individual cell is composed of its abundant functional molecules, and its integral interaction with the surrounding homogeneous or heterogeneous cells contributes to the whole functional organ.

The major biofunction of root nodules is symbiotic nitrogen fixation. The major ammonium assimilation product is asparagine in temperate legumes, such as *Medicago*, and ureides in tropical legumes, such as soybean (Udvardi and Poole, 2013). Ureide synthesis has been reported to occur in un-infected cells, and the assimilation products are then secreted to the xylem stream in soybean (Nguyen et al., 1985; Collier and Tegeder, 2012). Similarly, we were excited to find that the nodule-expressed asparagine synthetase coding genes, *MtAS1* and *MtAS2*, were preferentially expressed in UIC2, which is consistent with the data from Limpens et al. (2013) (Figure 6A), suggesting that part of the ammonium assimilation assembly line is also isolated from nitrogen fixation cells in indeterminate nodules. The particular expression patterns of AA transporters further support this theory, and help the AA products translocate to the aerial parts. The nitrogen fixation cells and un-infected cells work as two core production departments that collaborate with each other to process atmospheric nitrogen into asparagine (Figure 6D) and then hand over the products to the downstream departments for allocation (Figure 7C), guaranteeing the smooth operation of the entire nodule factory. The significance of un-infected cells embedding the nitrogen fixation zone is emphasized in this research, especially their significant roles in glutamate and asparagine synthesis, which are usually neglected.

Recently, a single-cell-type transcriptome profiling of the nodules of *L. japonicus* uncovered expression differences among genes in the infected cells and un-infected cells in the nitrogen fixation zone (Wang et al., 2022). Unlike this research, the nodule of *L. japonicus* is the determinate type with a simpler cell constitution, and the two main cell groups, infected and un-infected cells, were harvested by manual selection and then sequenced with high precision, sacrificing the integrity of the nodule cell populations to some extent. Similar to this research, two of the main AS coding genes were also enriched in un-infected cells. It may be a conserved mode in legumes that nitrogen assimilation is shared by infected and un-infected cells, possibly preventing the infected cells from being overworked.

Finally, we utilized the UCSC Cell Browser (Speir et al., 2021) for online data visualization ([www.medicagowang.com/scrna/](http://www.medicagowang.com/scrna/)) to obtain the expression data for genes of interest (supplemental methods). In conclusion, our research provides a wealth of data with novel techniques to aid in understanding the precise architecture of indeterminate nodules at the single-cell level,

## Molecular Plant

which is of great significance for understanding the underlying molecular basis of symbiosis and nitrogen fixation.

## METHODS

### Plant materials and growth conditions

The *M. truncatula* ecotype A17 was used for indeterminate nodule scRNA-seq experiments and hair root transformation. Seeds were immersed in 98% H<sub>2</sub>SO<sub>4</sub> for 8 min, washed 3 times, sterilized with 0.5% NaClO (0.05% Triton X-100) for 10 min, washed 5 times, and then laid on 0.8% agar and stored at 4°C in the dark for 3 days. The pretreated seeds were germinated at room temperature and then planted in the substrate or used for hairy root transformation. The greenhouse conditions were set to 16 h light/8 h dark with 22°C, 70%–80% humidity and 70–100 μmol m<sup>-2</sup> s<sup>-1</sup> light intensity.

### Rhizobia inoculation

Rhizobia inoculation referred to Zhu et al. (2020) and Laffont et al. (2020). For the wild-type A17, seedlings were planted in a vermiculite:perlite (5:2, v/v) mixture with N-deprived Fähraeus liquid medium for 7 days and then inoculated. For the hairy root-transformed plants, the N-starved period was extended to 10 days. For rhizobia inoculation, the wild-type *Sinorhizobium meliloti* 1021 (Sm1021) was used for scRNA-seq experiments and GUS reporter experiments, and Sm1021-RFP was used for fluorescent reporter experiments. Wild-type Sm1021 was cultured in TY medium with streptomycin (400 mg/l), and Sm1021-RFP was cultured in TY medium with streptomycin (400 mg/l) and tetracycline (10 mg/l). The culture conditions were 28°C in the dark. The rhizobia was suspended in N-deprived Fähraeus liquid medium to OD<sub>600</sub> of 0.05 for inoculation. Ten milliliters of the suspension was added to each seedling.

### Preparation of nodule protoplast samples for scRNA-seq

The 14-dpi pink nodules from 40 seedlings were collected for each sample. The nodules were first cut into ~1-mm slices and then immersed into fresh digestion solution (10 mM MES [pH 5.7], 3% [w/v] Cellulase RS, 2% [w/v] Macerozyme R10, 0.65 M mannitol, 20 mM KCl, 10 mM CaCl<sub>2</sub>, 2 mM MgCl<sub>2</sub>, 0.04% [w/v] pectolyase Y-23, 2% [w/v] hemicellulase, 10% [v/v] viscozyme, and 0.1% [w/v] BSA). The digestion reaction was carried out in the dark. The samples were placed at -0.09 MPa, maintained by a vacuum pump, for 15 min and then moved to a horizontal shaker at 50 rpm for 2 h. Microscopic examination was performed to ensure that the protoplast was evenly released when the sample was slightly squeezed. The samples were set aside for another 20 min, and then washed with wash solution (10 mM MES [pH 5.7], 10 mM CaCl<sub>2</sub>, 0.65 M mannitol, and 0.1% [w/v] BSA) and squeezed to help the protoplast release. The mixed sample was filtered with strainers twice (70 μm diameter the first time, 40 μm diameter the second time) to remove the tissue debris, and then the infected cells and un-infected cells were separated with a 20-μm strainer. The infected cells remaining on the filter were collected, washed with wash solution, and suspended in 50–100 μl of 0.65 M mannitol. The un-infected cells remaining in the filtrate were collected by concentration at 100 g for 5 min, and the supernatant was removed. The precipitate was suspended in 100 μl wash solution, and the mixture was gently moved onto sucrose flotation solution (10 mM MES [pH 5.7], 10 mM CaCl<sub>2</sub>, 25% [w/v] sucrose). Centrifugation at 100 g for 5 min was applied to settle the cell residue to the bottom. The supernatant with un-infected cells was collected and diluted with 10 volumes of wash solution. After concentration at 100 g for 5 min, the supernatant was removed, and the precipitate was suspended in 50–100 μl of 0.65 M mannitol. The infected and un-infected cells purified by the two separate steps were mixed and then processed for further sequencing experiments.

### scRNA-seq and raw data preprocessing

Approximately 8000–9000 counted cells were loaded for each independent library. The libraries were constructed based on Chromium Controller and Chromium Single Cell Reagent Kits v3 (10X Genomics, Pleasanton,

CA). Libraries were sequenced using an Illumina HiSeq 2500 platform (CapitalBio Technology, Beijing). The raw scRNA-seq dataset was first analyzed by Cell Ranger 3.1.0 (10X Genomics). Sequence reads were aligned to the *M. truncatula* reference genome (MtrunA17r5.0) with annotation r1.7. Then, the raw count matrix data were analyzed using the Seurat (v4.1.1) package.

To remove dead cells and doublets, the cells expressing fewer than 200 or over 6000 genes were removed; the genes expressed in fewer than 20 cells were removed; and the cells with more than 25% mitochondrial genes were removed. After filtering, 22 228 genes across 9756 cells in the two samples were used for further analysis.

### Cell clustering

Based on the Seurat (v4.1.1) package (Satija et al., 2015), “Find VariableFeatures” and “FindIntegrationAnchors” were applied to find the top variable genes shared in both samples, which were then used for PCA dimensional reduction. The first 20 PCs were selected for clustering with resolution parameters of 0.1, 0.2, 0.4, 0.6, 0.8, and 1.0. “Clutree” was applied for visualization of different clustering under differing resolutions. At a resolution of 0.4, the clusters were visualized and explored by t-SNE and UMAP. The function “FindAllMarkers” in the Seurat package was used to identify marker genes for all clusters. We also identified the DEGs between clusters with the “AverageExpression” function. “DoHeatmap” was applied to visualize the expression patterns of the top 20 marker genes/protoplasting-induced genes from each cluster. “FeaturePlot” and “VlnPlot” were used to visualize gene expression.

### Reconstruction of the cell differentiation trajectory

The Monocle 2 (v.2.22.0) R package was used to construct the cell differentiation trajectory. The subsets of raw data of particular cell types (NA2, PI, IF, and NF1 for the symbiotic group; NA1, NP, UIC1, UIC2, and VA for the un-symbiotic group) were used to explore the pseudotime developmental trajectory. First, we identified the variable genes based on the “dispersionTable” function ( $q < 0.001$ , 750 genes for the symbiotic group, 2300 genes for the un-symbiotic group). Then, the dimensional reduction clustering analysis was carried out with “reduceDimension” (set max\_components = 2, method = DDRTree). The state and pseudotime transition of cells was displayed by “orderCells.” “plot\_pseudotime\_heatmap” was used to cluster and visualize the top 50 DEGs along the trajectory. The “plot\_genes\_in\_pseudotime” was used to visualize the expression pattern of the specific gene. The Monocle 3 (v.1.2.9) package was applied to calculate and visualize the trajectory by UMAP.

### GO enrichment assay and pathway analysis

The top 100 marker genes (ranked by avg\_log2FC) in each cell cluster were extracted for the GO enrichment assay. The GO annotations were downloaded from <https://medicago.toulouse.inra.fr/MtrunA17r5.0-ANR/> (Pecrix et al., 2018). The R package ClusterProfiler was used for GO and pathway enrichment analysis. “compareCluster” was applied for enrichment (fun = “enricher,” pvalueCutoff = 0.01, pAdjustMethod = “BH,” qvalueCutoff = 0.005). For visualization in dotplot, we further set the threshold (number of enriched genes to total genes with GO annotation in the cluster)  $> 0.025$ .

### Construction of GUS reporter vectors and fluorescent reporter vectors

For GUS reporter vectors, we cloned 2.5–3 kb DNA sequences upstream of the start codon of each marker gene from the A17 genotype. The detailed promoter lengths and primers are listed in *Supplemental Table 13*. The promoter fragment was ligated by homologous recombination into pCAMBIA1381 digested with *Sall* and *HindIII* to fuse with the *GUS* gene.

For fluorescent reporter vectors, the coding sequences of *MtAS1* and *MtAS2* were cloned from A17 nodule cDNA and fused with *GFP* at the

3' terminus. *MtAS1-GFP* and *MtAS2-GFP* were ligated into *pCAMBIA1381-MtAS1* and *pCAMBIA1381-MtAS2* digested by *Ncol* and *PmlI*, replacing the original *GUS* gene, which resulted in *MtAS1 pro:MtAS1-GFP* and *MtAS2 pro:MtAS2-GFP*, respectively.

### Hairy root transformation

*Agrobacterium rhizogenes* strain ARqua1 was applied for hairy root transformation. The strain was transformed with the target binary vector by electroporation and selectively cultured on TY medium with streptomycin (400 mg/l) and kanamycin (50 mg/l) at 28°C in the dark. The positive clones were confirmed by PCR and sequencing and then used for the next-step infection. The germinated wild-type A17 was prepared by cutting off ~2/3 of the radicle under sterile condition, and then applying ARqua1 at the incision. The infected explant was laid on half-strength Murashige and Skoog medium (without sucrose) with 1.5% (w/v) agar for coculture at 20°C for a week, and then moved to half-strength Murashige and Skoog medium with 1.2% (w/v) sucrose, 1.2% (w/v) agar and 200 mg/l Timentin for hairy root development at 24°C for another week. Then, the transformed seedlings with hairy roots were moved to the substrate for further experiments.

### Fluorescence microscopy

Transgenic roots inoculated with Sm1021-RFP were collected at 28 dpi. Part of the roots were used for DNA extraction and transgene identification by PCR. Nodules from positive samples were embedded in 6% agarose, sliced into 80-μm sections using a VT1000S vibratome (Leica) and stained with DAPI (20 μg/ml, Sigma, D9542) solution. Fluorescence was captured via a Leica SP8 confocal microscope.

### GUS staining and microscopy

Transgenic roots with nodules were collected at 21 dpi and incubated in GUS staining solution (50 mM phosphate buffer [pH 7.0], 5 mM potassium ferricyanide, 5 mM potassium ferrocyanide, 1 mM X-Gluc), and vacuumed to  $-0.09$  MPa three times in the dark for 30 min each time. Staining lasted another 6 h at 37°C in the dark. Then, the samples were washed with 75% ethanol three times for 6 h each time. The nodules were embedded in 6% agarose, sliced into 80-μm sections using a VT1000S vibratome (Leica), and photographed with an Olympus BX53.

## DATA AVAILABILITY

The scRNA-seq data generated in this study have been deposited with the China National Genomics Data Center with BioProject number PRJCA012129 and can also be visualized via <http://www.medicagowang.com/scrna/>.

## SUPPLEMENTAL INFORMATION

Supplemental information is available at *Molecular Plant Online*.

## FUNDING

This research was funded by National Key Research & Development Program of China (2022YFA0912100), National Natural Science Foundation of China (32070272), and Key Projects in Science and Technology of Inner Mongolia (2021ZD0031).

## AUTHOR CONTRIBUTIONS

T.W. and J.D. conceived of the study. Q.Y. and F.Z. designed the experiments. Q.Y., F.Z., F.S., T.-C.W., J.W., P.L., and C.S. performed the experiments and analyzed the data. Q.Y., F.Z., J.D., and T.W. wrote the manuscript.

## ACKNOWLEDGMENTS

We thank CapitalBio Technology (Beijing) for providing sequencing service. No conflict of interest declared.

Received: March 15, 2022  
 Revised: August 30, 2022  
 Accepted: October 23, 2022  
 Published: October 28, 2022

## REFERENCES

- Allen, T., Raja, S., and Dunn, K.** (1991). Cells expressing ENOD2 show differential spatial organization during the development of alfalfa root nodules. *Mol. Plant Microbe Interact.* **4**:139–146. <https://doi.org/10.1094/mpmi-4-139>.
- Alunni, B., Kevei, Z., Redondo-Nieto, M., Kondorosi, A., Mergaert, P., and Kondorosi, E.** (2007). Genomic organization and evolutionary insights on GRP and NCR genes, two large nodule-specific gene families in *Medicago truncatula*. *Mol. Plant Microbe Interact.* **20**:1138–1148. <https://doi.org/10.1094/mpmi-20-9-1138>.
- Bauchrowitz, M.A., Barker, D.G., and Truchet, G.** (1996). Lectin genes are expressed throughout root nodule development and during nitrogen-fixation in the Rhizobium-Medicago symbiosis. *Plant J.* **9**:31–43. <https://doi.org/10.1046/j.1365-313X.1996.09010031.x>.
- Birnbaum, K., Shasha, D.E., Wang, J.Y., Jung, J.W., Lambert, G.M., Galbraith, D.W., and Benfey, P.N.** (2003). A gene expression map of the *Arabidopsis* root. *Science* **302**:1956–1960. <https://doi.org/10.1126/science.1090022>.
- Buer, C.S., Imin, N., and Djordjevic, M.A.** (2010). Flavonoids: new roles for old molecules. *J. Integr. Plant Biol.* **52**:98–111. <https://doi.org/10.1111/j.1744-7909.2010.00905.x>.
- Cao, J., Spielmann, M., Qiu, X., Huang, X., Ibrahim, D.M., Hill, A.J., Zhang, F., Mundlos, S., Christiansen, L., Steemers, F.J., et al.** (2019). The single-cell transcriptional landscape of mammalian organogenesis. *Nature* **566**:496–502. <https://doi.org/10.1038/s41586-019-0969-x>.
- Carvalho, H.G., Lopes-Cardoso, I.A., Lima, L.M., Melo, P.M., and Cullimore, J.V.** (2003). Nodule-specific modulation of glutamine synthetase in transgenic *Medicago truncatula* leads to inverse alterations in asparagine synthetase expression. *Plant Physiol.* **133**:243–252. <https://doi.org/10.1104/pp.102.017830>.
- Cerri, M.R., Frances, L., Laloum, T., Auriac, M.C., Niebel, A., Oldroyd, G.E.D., Barker, D.G., Fournier, J., and de Carvalho-Niebel, F.** (2012). Medicago truncatula ERN transcription factors: regulatory interplay with NSP1/NSP2 GRAS factors and expression dynamics throughout rhizobial infection. *Plant Physiol.* **160**:2155–2172. <https://doi.org/10.1104/pp.112.203190>.
- Collier, R., and Tegeder, M.** (2012). Soybean ureide transporters play a critical role in nodule development, function and nitrogen export. *Plant J.* **72**:355–367. <https://doi.org/10.1111/j.1365-313X.2012.05086.x>.
- Combier, J.-P., Vernié, T., de Billy, F., El Yahyaoui, F., Mathis, R., and Gamas, P.** (2007). The MtMMPL1 early nodulin is a novel member of the matrix metalloendoproteinase family with a role in *Medicago truncatula* infection by *Sinorhizobium meliloti*. *Plant Physiol.* **144**:703–716. <https://doi.org/10.1104/pp.106.092585>.
- de Bang, T.C., Lundquist, P.K., Dai, X., Boschiero, C., Zhuang, Z., Pant, P., Torres-Jerez, I., Roy, S., Nogales, J., Veerappan, V., et al.** (2017). Genome-wide identification of *Medicago* peptides involved in macronutrient responses and nodulation. *Plant Physiol.* **175**:1669–1689. <https://doi.org/10.1104/pp.17.01096>.
- Denyer, T., Ma, X., Klesen, S., Scacchi, E., Niesel, K., and Timmermans, M.C.P.** (2019). Spatiotemporal developmental trajectories in the *Arabidopsis* root revealed using high-throughput single-cell RNA sequencing. *Dev. Cell* **48**:840–852.e5. <https://doi.org/10.1016/j.devcel.2019.02.022>.
- Dinkeloo, K., Boyd, S., and Pilot, G.** (2018). Update on amino acid transporter functions and on possible amino acid sensing mechanisms in plants. *Semin. Cell Dev. Biol.* **74**:105–113. <https://doi.org/10.1016/j.semcd.2017.07.010>.
- El Yahyaoui, F., Küster, H., Ben Amor, B., Hohnjec, N., Pühler, A., Becker, A., Gouzy, J., Vernié, T., Gough, C., Niebel, A., et al.** (2004). Expression profiling in *Medicago truncatula* identifies more than 750 genes differentially expressed during nodulation, including many potential regulators of the symbiotic program. *Plant Physiol.* **136**:3159–3176. <https://doi.org/10.1104/pp.104.043612>.
- Farkas, A., Maróti, G., Durgó, H., György, Z., Lima, R.M., Medzihardszky, K.F., Kereszt, A., Mergaert, P., and Kondorosi, É.** (2014). *Medicago truncatula* symbiotic peptide NCR247 contributes to bacteroid differentiation through multiple mechanisms. *Proc. Natl. Acad. Sci. USA* **111**:5183–5188. <https://doi.org/10.1073/pnas.1404169111>.
- Forde, B.G., and Lea, P.J.** (2007). Glutamate in plants: metabolism, regulation, and signalling. *J. Exp. Bot.* **58**:2339–2358. <https://doi.org/10.1093/jxb/erm121>.
- Franssen, H.J., Xiao, T.T., Kulikova, O., Wan, X., Bisseling, T., Scheres, B., and Heidstra, R.** (2015). Root developmental programs shape the *Medicago truncatula* nodule meristem. *Development* **142**:2941–2950. <https://doi.org/10.1242/dev.120774>.
- Gamas, P., de Billy, F., and Truchet, G.** (1998). Symbiosis-specific expression of two *Medicago truncatula* nodulin genes, MtN1 and MtN13, encoding products homologous to plant defense proteins. *Mol. Plant Microbe Interact.* **11**:393–403. <https://doi.org/10.1094/mpmi.1998.11.5.393>.
- Gamas, P., Niebel, F.d.C., Lescure, N., and Cullimore, J.** (1996). Use of a subtractive hybridization approach to identify new *Medicago truncatula* genes induced during root nodule development. *Mol. Plant Microbe Interact.* **9**:233–242. <https://doi.org/10.1094/mpmi-9-0233>.
- Gifford, I., Battenberg, K., Vaniya, A., Wilson, A., Tian, L., Fiehn, O., and Berry, A.M.** (2018). Distinctive patterns of flavonoid biosynthesis in roots and nodules of *Datisca glomerata* and *Medicago* spp. revealed by metabolomic and gene expression profiles. *Front. Plant Sci.* **9**:1463. <https://doi.org/10.3389/fpls.2018.01463>.
- Godiard, L., Lepage, A., Moreau, S., Laporte, D., Verdeneaud, M., Timmers, T., and Gamas, P.** (2011). MtbHLH1, a bHLH transcription factor involved in *Medicago truncatula* nodule vascular patterning and nodule to plant metabolic exchanges. *New Phytol.* **191**:391–404. <https://doi.org/10.1111/j.1469-8137.2011.03718.x>.
- Guenoune, D., Galili, S., Phillips, D.A., Volpin, H., Chet, I., Okon, Y., and Kapulnik, Y.** (2001). The defense response elicited by the pathogen *Rhizoctonia solani* is suppressed by colonization of the AM-fungus *Glomus intraradices*. *Plant Sci.* **160**:925–932. [https://doi.org/10.1016/S0168-9452\(01\)00329-6](https://doi.org/10.1016/S0168-9452(01)00329-6).
- Jean-Baptiste, K., McFainé-Figueroa, J.L., Alexandre, C.M., Dorrrity, M.W., Saunders, L., Bubb, K.L., Trapnell, C., Fields, S., Queitsch, C., and Cuperus, J.T.** (2019). Dynamics of gene expression in single root cells of *Arabidopsis thaliana*. *Plant Cell* **31**:993–1011. <https://doi.org/10.1105/tpc.18.00785>.
- Jia, N., Zhu, Y., and Xie, F.** (2018). An efficient protocol for model legume root protoplast isolation and transformation. *Front. Plant Sci.* **9**:670. <https://doi.org/10.3389/fpls.2018.00670>.
- Jiang, S., Jardinaud, M.F., Gao, J., Pecrix, Y., Wen, J., Mysore, K., Xu, P., Sanchez-Canizares, C., Ruan, Y., Li, Q., et al.** (2021). NIN-like protein transcription factors regulate leghemoglobin genes in legume nodules. *Science* **374**:625–628. <https://doi.org/10.1126/science.abg5945>.
- Journet, E.P., El-Gachoui, N., Vernoud, V., de Billy, F., Pichon, M., Dedieu, A., Arnould, C., Morandi, D., Barker, D.G., and Gianinazzi-Pearson, V.** (2001). *Medicago truncatula* ENOD11: a novel RPRP-encoding early nodulin gene expressed during mycorrhization in arbuscule-containing cells. *Mol. Plant Microbe Interact.* **14**:737–748. <https://doi.org/10.1094/MPMI.2001.14.6.737>.

- Kolodziejczyk, A.A., Kim, J.K., Svensson, V., Marioni, J.C., and Teichmann, S.A.** (2015). The technology and biology of single-cell RNA sequencing. *Mol. Cell* **58**:610–620. <https://doi.org/10.1016/j.molcel.2015.04.005>.
- Laffont, C., Ivanovici, A., Gautrat, P., Brault, M., Djordjevic, M.A., and Frugier, F.** (2020). The NIN transcription factor coordinates CEP and CLE signaling peptides that regulate nodulation antagonistically. *Nat. Commun.* **11**:3167. <https://doi.org/10.1038/s41467-020-16968-1>.
- Larrañzar, E., Riely, B.K., Kim, S.C., Carrasquilla-Garcia, N., Yu, H.J., Hwang, H.J., Oh, M., Kim, G.B., Surendraraao, A.K., Chasman, D., et al.** (2015). Deep sequencing of the *Medicago truncatula* root transcriptome reveals a massive and early interaction between nodulation factor and ethylene signals. *Plant Physiol.* **169**:233–265. <https://doi.org/10.1104/pp.15.00350>.
- Limpens, E., Mirabella, R., Fedorova, E., Franken, C., Franssen, H., Bisseling, T., and Geurts, R.** (2005). Formation of organelle-like N<sub>2</sub>-fixing symbiosomes in legume root nodules is controlled by DMI2. *Proc. Natl. Acad. Sci. USA* **102**:10375–10380. <https://doi.org/10.1073/pnas.0504284102>.
- Limpens, E., Moling, S., Hooiveld, G., Pereira, P.A., Bisseling, T., Becker, J.D., and Küster, H.** (2013). Cell- and tissue-specific transcriptome analyses of *Medicago truncatula* root nodules. *PLoS One* **8**, e64377. <https://doi.org/10.1371/journal.pone.0064377>.
- Liu, C.-W., and Murray, J.D.** (2016). The role of flavonoids in nodulation host-range specificity: an update. *Plants* **5**:33. <https://doi.org/10.3390/plants5030033>.
- Liu, C.W., Breakspear, A., Guan, D., Cerri, M.R., Jackson, K., Jiang, S., Robson, F., Radhakrishnan, G.V., Roy, S., Bone, C., et al.** (2019). NIN acts as a network hub controlling a growth module required for rhizobial infection. *Plant Physiol.* **179**:1704–1722. <https://doi.org/10.1104/pp.18.01572>.
- Liu, J., Miller, S.S., Graham, M., Bucciarelli, B., Catalano, C.M., Sherrier, D.J., Samac, D.A., Ivashuta, S., Fedorova, M., Matsumoto, P., et al.** (2006). Recruitment of novel calcium-binding proteins for root nodule symbiosis in *Medicago truncatula*. *Plant Physiol.* **141**:167–177. <https://doi.org/10.1104/pp.106.076711>.
- Liu, Q., Liang, Z., Feng, D., Jiang, S., Wang, Y., Du, Z., Li, R., Hu, G., Zhang, P., Ma, Y., et al.** (2021). Transcriptional landscape of rice roots at the single-cell resolution. *Mol. Plant* **14**:384–394. <https://doi.org/10.1016/j.molp.2020.12.014>.
- Liu, Z., Zhou, Y., Guo, J., Li, J., Tian, Z., Zhu, Z., Wang, J., Wu, R., Zhang, B., Hu, Y., et al.** (2020). Global dynamic molecular profiles of stomatal lineage cell development by single-cell RNA sequencing. *Mol. Plant* **13**:1178–1193. <https://doi.org/10.1016/j.molp.2020.06.010>.
- Maia, L.G.S.** (2018). Involvement of Two Novel GRF-Type Zinc Finger Nodulins During Rhizobial Symbiotic Establishment in *Medicago Truncatula* Nodules. Graduate Theses, Dissertations, and Problem Reports (Morgantown, West Virginia: West Virginia University), 6142. <https://researchrepository.wvu.edu/etd/6142>.
- Marino, D., Andrio, E., Danchin, E.G.J., Oger, E., Guciardo, S., Lambert, A., Puppo, A., and Pauly, N.** (2011). A *Medicago truncatula* NADPH oxidase is involved in symbiotic nodule functioning. *New Phytol.* **189**:580–592. <https://doi.org/10.1111/j.1469-8137.2010.03509.x>.
- Mathis, R., Grosjean, C., de Billy, F., Huguet, T., and Gamas, P.** (1999). The early nodulin gene MtN6 is a novel marker for events preceding infection of *Medicago truncatula* roots by *Sinorhizobium meliloti*. *Mol. Plant Microbe Interact.* **12**:544–555. <https://doi.org/10.1094/mpmi.1999.12.6.544>.
- Maxwell, C.A., Hartwig, U.A., Joseph, C.M., and Phillips, D.A.** (1989). A chalcone and two related flavonoids released from alfalfa roots induce nod genes of *Rhizobium meliloti*. *Plant Physiol.* **91**:842–847. <https://doi.org/10.1104/pp.91.3.842>.
- Nguyen, T., Zelechowska, M., Foster, V., Bergmann, H., and Verma, D.P.** (1985). Primary structure of the soybean Nodulin-35 gene encoding uricase-II localized in the peroxisomes of uninfected cells of nodules. *Proc. Natl. Acad. Sci. USA* **82**:5040–5044. <https://doi.org/10.1073/pnas.82.15.5040>.
- Niebel, F.d.C., Lescure, N., Cullimore, J.V., and Gamas, P.** (1998). The *Medicago truncatula* MtAnn1 gene encoding an annexin is induced by Nod factors and during the symbiotic interaction with *Rhizobium meliloti*. *Mol. Plant Microbe Interact.* **11**:504–513. <https://doi.org/10.1094/mpmi.1998.11.6.504>.
- Ott, T., van Dongen, J.T., Günther, C., Krusell, L., Desbrosses, G., Vigeolas, H., Bock, V., Czechowski, T., Geigenberger, P., and Udvardi, M.K.** (2005). Symbiotic leghemoglobins are crucial for nitrogen fixation in legume root nodules but not for general plant growth and development. *Curr. Biol.* **15**:531–535. <https://doi.org/10.1016/j.cub.2005.01.042>.
- Pecrix, Y., Staton, S.E., Sallet, E., Lelandais-Brière, C., Moreau, S., Carrère, S., Blein, T., Jardinaud, M.F., Latrasse, D., Zouine, M., et al.** (2018). Whole-genome landscape of *Medicago truncatula* symbiotic genes. *Nat. Plants* **4**:1017–1025. <https://doi.org/10.1038/s41477-018-0286-7>.
- Pichon, M., Journet, E.P., Dedieu, A., de Billy, F., Truchet, G., and Barker, D.G.** (1992). *Rhizobium meliloti* elicits transient expression of the early nodulin gene ENOD12 in the differentiating root epidermis of transgenic alfalfa. *Plant Cell* **4**:1199–1211. <https://doi.org/10.1105/tpc.4.10.1199>.
- Pilot, G., Stransky, H., Bushey, D.F., Pratelli, R., Ludewig, U., Wingate, V.P.M., and Frommer, W.B.** (2004). Overexpression of GLUTAMINE DUMPER1 leads to hypersecretion of glutamine from *Hydathodes* of *Arabidopsis* leaves. *Plant Cell* **16**:1827–1840. <https://doi.org/10.1105/tpc.021642>.
- Qiu, X., Mao, Q., Tang, Y., Wang, L., Chawla, R., Pliner, H.A., and Trapnell, C.** (2017). Reversed graph embedding resolves complex single-cell trajectories. *Nat. Methods* **14**:979–982. <https://doi.org/10.1038/nmeth.4402>.
- Rentsch, D., Schmidt, S., and Tegeder, M.** (2007). Transporters for uptake and allocation of organic nitrogen compounds in plants. *FEBS Lett.* **581**:2281–2289. <https://doi.org/10.1016/j.febslet.2007.04.013>.
- Roux, B., Rodde, N., Jardinaud, M.-F., Timmers, T., Sauviac, L., Cottret, L., Carrère, S., Sallet, E., Courcelle, E., Moreau, S., et al.** (2014). An integrated analysis of plant and bacterial gene expression in symbiotic root nodules using laser-capture microdissection coupled to RNA sequencing. *Plant J.* **77**:817–837. <https://doi.org/10.1111/tpj.12442>.
- Roy, S., Liu, W., Nandety, R.S., Crook, A., Mysore, K.S., Pislaru, C.I., Frugoli, J., Dickstein, R., and Udvardi, M.K.** (2020). Celebrating 20 years of genetic discoveries in legume nodulation and symbiotic nitrogen fixation. *Plant Cell* **32**:15–41. <https://doi.org/10.1105/tpc.19.00279>.
- Ryu, K.H., Huang, L., Kang, H.M., and Schiefelbein, J.** (2019). Single-cell RNA sequencing resolves molecular relationships among individual plant cells. *Plant Physiol.* **179**:1444–1456. <https://doi.org/10.1104/pp.18.01482>.
- Satgé, C., Moreau, S., Sallet, E., Lefort, G., Auriac, M.-C., Remblière, C., Cottret, L., Gallardo, K., Noirot, C., Jardinaud, M.-F., et al.** (2016). Reprogramming of DNA methylation is critical for nodule development in *Medicago truncatula*. *Nat. Plants* **2**, 16166. <https://doi.org/10.1038/nplants.2016.166>.
- Satija, R., Farrell, J.A., Gennert, D., Schier, A.F., and Regev, A.** (2015). Spatial reconstruction of single-cell gene expression data. *Nat. Biotechnol.* **33**:495–502. <https://doi.org/10.1038/nbt.3192>.

## Single-cell transcriptome in *Medicago* nodules

## Molecular Plant

- Saur, I.M.L., Oakes, M., Djordjevic, M.A., and Imlim, N.** (2011). Crosstalk between the nodulation signaling pathway and the autoregulation of nodulation in *Medicago truncatula*. *New Phytol.* **190**:865–874. <https://doi.org/10.1111/j.1469-8137.2011.03738.x>.
- Schiessl, K., Lilley, J.L.S., Lee, T., Tamvakis, I., Kohlen, W., Bailey, P.C., Thomas, A., Luptak, J., Ramakrishnan, K., Carpenter, M.D., et al.** (2019). NODULE INCEPTION recruits the lateral root developmental program for symbiotic nodule organogenesis in *Medicago truncatula*. *Curr. Biol.* **29**:3657–3668.e5. <https://doi.org/10.1016/j.cub.2019.09.005>.
- Selker, J.M., and Newcomb, E.H.** (1985). Spatial relationships between uninfected and infected-cells in root-nodules of soybean. *Planta* **165**:446–454. <https://doi.org/10.1007/bf00398089>.
- Senovilla, M., Castro-Rodríguez, R., Abreu, I., Escudero, V., Kryvoruchko, I., Udvardi, M.K., Imperial, J., and González-Guerrero, M.** (2018). *Medicago truncatula* copper transporter 1 (MtCOPT1) delivers copper for symbiotic nitrogen fixation. *New Phytol.* **218**:696–709. <https://doi.org/10.1111/nph.14992>.
- Shaw, R., Tian, X., and Xu, J.** (2021). Single-cell transcriptome analysis in plants: advances and challenges. *Mol. Plant* **14**:115–126. <https://doi.org/10.1016/j.molp.2020.10.012>.
- Silva-Navas, J., Moreno-Risueno, M.A., Manzano, C., Téllez-Robledo, B., Navarro-Neila, S., Carrasco, V., Pollmann, S., Gallego, F.J., and del Pozo, J.C.** (2016). Flavonols mediate root phototropism and growth through regulation of proliferation-to-differentiation transition. *Plant Cell* **28**:1372–1387. <https://doi.org/10.1105/tpc.15.00857>.
- Speir, M.L., Bhaduri, A., Markov, N.S., Moreno, P., Nowakowski, T.J., Papatheodorou, I., Pollen, A.A., Raney, B.J., Seninge, L., Kent, W.J., et al.** (2021). UCSC Cell Browser: visualize your single-cell data. *Bioinformatics* **37**:4578–4580. <https://doi.org/10.1093/bioinformatics/btab503>.
- Sprent, J.I.** (2007). Evolving ideas of legume evolution and diversity: a taxonomic perspective on the occurrence of nodulation. *New Phytol.* **174**:11–25. <https://doi.org/10.1111/j.1469-8137.2007.02015.x>.
- Stacey, G.** (2007). Chapter 10 - the rhizobium-legume nitrogen-fixing symbiosis. In *Biology of the Nitrogen Cycle*, H. Bothe, S.J. Ferguson, and W.E. Newton, eds. (Amsterdam: Elsevier), pp. 147–163. <https://doi.org/10.1016/B978-044452857-5.50011-4>.
- Ta, T.C., Faris, M.A., and Macdowall, F.D.** (1986). Pathways of nitrogen metabolism in nodules of alfalfa (*Medicago sativa* L.). *Plant Physiol.* **80**:1002–1005. <https://doi.org/10.1104/pp.80.4.1002>.
- Tegeder, M., and Ward, J.M.** (2012). Molecular evolution of plant AAP and LHT amino acid transporters. *Front. Plant Sci.* **3**:21. <https://doi.org/10.3389/fpls.2012.00021>.
- Temple, S.J., Vance, C.P., and Stephen Gantt, J.** (1998). Glutamate synthase and nitrogen assimilation. *Trends Plant Sci.* **3**:51–56. [https://doi.org/10.1016/S1360-1385\(97\)01159-X](https://doi.org/10.1016/S1360-1385(97)01159-X).
- Tesfaye, M., Samac, D.A., and Vance, C.P.** (2006). Insights into symbiotic nitrogen fixation in *Medicago truncatula*. *Mol. Plant Microbe Interact.* **19**:330–341. <https://doi.org/10.1094/mpmi-19-0330>.
- Udvardi, M., and Poole, P.S.** (2013). Transport and metabolism in legume-rhizobia symbioses. *Annu. Rev. Plant Biol.* **64**:781–805. <https://doi.org/10.1146/annurev-arplant-050312-120235>.
- van de Wiel, C., Scheres, B., Franssen, H., van Lierop, M.J., van Lammeren, A., van Kammen, A., and Bisseling, T.** (1990). The early nodulin transcript ENOD2 is located in the nodule parenchyma (inner cortex) of pea and soybean root nodules. *EMBO J.* **9**:1–7. <https://doi.org/10.1002/j.1460-2075.1990.tb08073.x>.
- Vasse, J., Debilly, F., Camut, S., and Truchet, G.** (1990). Correlation between ultrastructural differentiation of bacteroids and nitrogen-fixation in alfalfa nodules. *J. Bacteriol.* **172**:4295–4306. <https://doi.org/10.1128/jb.172.8.4295-4306.1990>.
- Vernié, T., Moreau, S., de Billy, F., Plet, J., Combier, J.P., Rogers, C., Oldroyd, G., Frugier, F., Niebel, A., and Gamas, P.** (2008). EFD1 is an ERF transcription factor involved in the control of nodule number and differentiation in *Medicago truncatula*. *Plant Cell* **20**:2696–2713. <https://doi.org/10.1105/tpc.108.059857>.
- Wang, D., Griffitts, J., Starker, C., Fedorova, E., Limpens, E., Ivanov, S., Bisseling, T., and Long, S.** (2010). A nodule-specific protein secretory pathway required for nitrogen-fixing symbiosis. *Science* **327**:1126–1129. <https://doi.org/10.1126/science.1184096>.
- Wang, L., Zhou, Y., Li, R., Liang, J., Tian, T., Ji, J., Chen, R., Zhou, Y., Fan, Q., Ning, G., et al.** (2022). Single cell-type transcriptome profiling reveals genes that promote nitrogen fixation in the infected and uninfected cells of legume nodules. *Plant Biotechnol. J.* **20**:616–618. <https://doi.org/10.1111/pbi.13778>.
- Xiao, T.T., Schilderink, S., Moling, S., Deinum, E.E., Kondorosi, E., Franssen, H., Kulikova, O., Niebel, A., and Bisseling, T.** (2014). Fate map of *Medicago truncatula* root nodules. *Development* **141**:3517–3528. <https://doi.org/10.1242/dev.110775>.
- Yang, H., Postel, S., Kemmerling, B., and Ludewig, U.** (2014). Altered growth and improved resistance of *Arabidopsis* against *Pseudomonas syringae* by overexpression of the basic amino acid transporter AtCAT1. *Plant Cell Environ.* **37**:1404–1414. <https://doi.org/10.1111/pce.12244>.
- Zhang, T.Q., Chen, Y., and Wang, J.W.** (2021a). A single-cell analysis of the *Arabidopsis* vegetative shoot apex. *Dev. Cell* **56**:1056–1074.e8. <https://doi.org/10.1016/j.devcel.2021.02.021>.
- Zhang, T.Q., Xu, Z.G., Shang, G.D., and Wang, J.W.** (2019). A single-cell RNA sequencing profiles the developmental landscape of *Arabidopsis* root. *Mol. Plant* **12**:648–660. <https://doi.org/10.1016/j.molp.2019.04.004>.
- Zhang, T.Q., Chen, Y., Liu, Y., Lin, W.H., and Wang, J.W.** (2021b). Single-cell transcriptome atlas and chromatin accessibility landscape reveal differentiation trajectories in the rice root. *Nat. Commun.* **12**:2053. <https://doi.org/10.1038/s41467-021-22352-4>.
- Zhao, C., Pratelli, R., Yu, S., Shelley, B., Collakova, E., and Pilot, G.** (2021). Detailed characterization of the UMAMIT proteins provides insight into their evolution, amino acid transport properties, and role in the plant. *J. Exp. Bot.* **72**:6400–6417. <https://doi.org/10.1093/jxb/erab288>.
- Zhu, F., Deng, J., Chen, H., Liu, P., Zheng, L., Ye, Q., Li, R., Brault, M., Wen, J., Frugier, F., et al.** (2020). A CEP peptide receptor-like kinase regulates auxin biosynthesis and ethylene signaling to coordinate root growth and symbiotic nodulation in *Medicago truncatula*. *Plant Cell* **32**:2855–2877. <https://doi.org/10.1105/tpc.20.00248>.
- Zuanazzi, J.A.S., Clergeot, P.H., Quirion, J.C., Husson, H.P., Kondorosi, A., and Ratet, P.** (1998). Production of *Sinorhizobium meliloti* nod gene activator and repressor flavonoids from *Medicago sativa* roots. *Mol. Plant Microbe Interact.* **11**:784–794. <https://doi.org/10.1094/Mpmi.1998.11.8.784>.